ELSEVIER

Agricultural and Forest Meteorology 93 (1999) 211–228

AGRICULTURAL AND FOREST METEOROLOGY

An improved algorithm for estimating incident daily solar radiation from measurements of temperature, humidity, and precipitation

Peter E. Thornton*, Steven W. Running

Numerical Terradynamics Simulation Group, School of Forestry, The University of Montana, Missoula, MT 59812, USA

Received 27 July 1998; accepted 9 November 1998

Abstract

We present a reformulation of the Bristow–Campbell model for daily solar radiation, developed using daily observations of radiation, temperature, humidity, and precipitation, from 40 stations in contrasting climates. By expanding the original model to include a spatially and temporally variable estimate of clear-sky transmittance, and applying a small number of other minor modifications, the new model produces better results than the original over a wider range of climates. Our method does not require reparameterization on a site-by-site basis, a distinct advantage over the original approach. We do require observations of dewpoint temperature, which the original model does not, but we suggest a method that could eliminate this dependency. Mean absolute error (MAE) for predictions of clear-sky transmittance was improved by 28% compared to the original model formulation. Aerosols and snowcover probably contribute to variation in clear-sky transmittance that remains unexplained by our method. MAE and bias for prediction of daily incident radiation were about 2.4 MJ m^{-2} day^{-1} and +0.5 MJ m^{-2} day^{-1}, respectively. As a percent of the average observed values of incident radiation, MAE and bias are about 15% and +4%, respectively. The lowest errors and smallest biases (percent basis) occurred during the summer. The highest prediction biases were associated with stations having a strong seasonal concentration of precipitation, with underpredictions at summer-precipitation stations, and overpredictions at winter-precipitation stations. Further study is required to characterize the behavior of this method for tropical climates.

Keywords: Solar radiation; Atmospheric transmittance; Daily; Air temperature; Humidity; Snowcover; Ecosystem process simulation

1. Introduction

A lack of short-wave radiation observations has been a persistent problem in studies of land-surface processes. The number of surface weather stations recording daily radiation is very small compared to the number recording temperature and precipitation. In the United States, to take a best-case example, the ratio between stations observing radiation and those observing temperature is no better than 1:100 (NREL, 1993; NCDC, 1995), and globally the ratio may be as low as 1:500. The need for a general method for estimating incident radiation from commonly available inputs has grown as the spatial scope of research into land-surface processes has expanded from local, to regional, continental, and global scales.

Geostationary satellites can provide estimates of incident radiation over large regions, and while studies

*Corresponding author. Tel.: +1-406-243-4326; fax: +1-406-243-4510; e-mail: peter@ntsg.umt.edu

0168-1923/99/$ – see front matter
PII: S0168-1923(98)00126-9

have demonstrated the utility of these methods for daily predictions over areas as small as 150 km^2 (Kustas et al., 1994), they have been tested mostly for monthly estimation over large areas (1° by 1° or larger grid-cells, Pinker et al., 1995). Regardless of the accuracy of these methods, they have limited utility in the construction of historical databases.

Bristow and Campbell (1984) (hereafter denoted B&C) demonstrated that a relationship exists between the diurnal range in near-surface air temperature and the daily total solar radiation incident at the surface. They developed and tested their method (hereafter denoted M1) using data from three stations in the northwestern United States and showed that it provided accurate and relatively unbiased estimates of daily total radiation at these locations. They also noted that a more comprehensive study covering a wider range of climates would be required to test the general applicability of the method. M1 has been used in numerous other studies (Running et al., 1987; Glassy and Running, 1994; Thornton et al., 1997), but a more exhaustive test using data from diverse climates has not been published.

The demand for land-surface radiation estimates is demonstrated by several recent research efforts. VEMAP (Vegetation/ecosystem modeling and analysis project) (Kittel et al., 1995; VEMAP Members, 1995), an ongoing intercomparison of land-surface process simulation models, used a variant of M1 to generate daily radiation values for 1 year on a 0.5° longitude/latitude grid over the conterminous U.S. A second phase of the project has expanded that application to cover a 99-year period, using historical observations of temperature and precipitation, and again incorporating a variant of M1 to arrive at estimates of daily incident radiation (Kittel et al., 1997). Hunt et al. (1996), in a study relating globally distributed point observations of atmospheric CO_2 concentration to simulated distributions of carbon sources and sinks, used a variant of M1 driven by gridded temperature and precipitation data (Piper, 1995) to produce a global 1° longitude/latitude grid of radiation values for a single year. A reassessment of M1 using observations from an expanded range of climates could benefit such studies by documenting model performance under different climates, and by providing a general and objective parameterization scheme.

Here we pursue a refinement of M1, using meteorological observations from the Solar and Meteorological Surface Observation Network (SAMSON) database (NREL, 1993). The SAMSON database includes hourly observations of radiation, temperature, humidity, and precipitation from stations in the United States with tropical, subtropical, warm-temperate, and cold-temperate climates. Our goal is a parameterization scheme that gives accurate results at stations with different climates without refitting model parameters on a case-by-case basis. We retain the general logic of M1, expanding it in some respects for the sake of improved accuracy, and extending the range of climates over which it gives useful predictions of daily total incident radiation.

2. Methods

2.1. Database generation

All data used are from the SAMSON database. SAMSON includes both observed and modeled hourly radiation values. We extracted hourly data for the period 1961–1990 for all stations with observed radiation values (the SAMSON first-order stations). For each hourly period we retrieved the following parameters: hourly potential radiation ($R_{pot,h}$), hourly global horizontal radiation, hourly dry bulb temperature, hourly dewpoint temperature, and hourly accumulated precipitation. Quality control flags for each parameter were extracted, as were longitude, latitude, and elevation for each station.

The hourly database was processed to create a daily database of: daily total potential radiation (R_{pot}, MJ m^{-2} day^{-1}), daily total global horizontal radiation (R_{gh}, MJ m^{-2} day^{-1}), daily maximum temperature (T_{max}, °C), daily minimum temperature (T_{min}, °C), daily average dewpoint temperature (T_{dew}, °C), and daily total precipitation (Q, mm day^{-1}). We eliminated all station-days with missing or modeled hourly radiation values for hours with $R_{pot,h} > 0$. Any station-day with any of its hourly temperature or precipitation data flagged as missing or corrupt in the original database was also marked as missing for the appropriate parameter in the daily database. After filtering, 40 stations having greater than 100 daily observations of R_{gh} remained (Table 1).

Table 1
Summary data for included SAMSON stations

Station	Köppen climate code[a]	Annual mean T_{air} (°C)	Annual total precipitation (cm)	Longitude (°W)	Latitude (°N)	Elevation (m)
Albany, NY	Df	8.6	91	73.80	42.75	89
Albuquerque, NM	BS	13.3	22	106.62	35.05	1619
Bismarck, ND	Df	5.6	39	100.75	46.77	502
Boise, ID	BS	10.6	30	116.22	43.57	874
Boston, MA	Cf	10.5	105	71.03	42.37	5
Boulder, CO	Cf	10.0	46	105.25	40.02	1634
Brownsville, TX	Cw	22.8	67	97.43	25.90	6
Burlington, VT	Df	7.1	87	73.15	44.47	104
Cape Hatteras, NC	Cf	16.8	142	75.55	35.27	2
Caribou, ME	Df	4.1	92	68.02	46.87	190
Charleston, SC	Cf	18.0	130	80.03	32.90	12
Columbia, MO	Cf	12.2	102	92.22	38.82	270
Daytona Beach, FL	Cf	21.0	121	81.05	29.18	12
Dodge City, KS	Cf	12.5	54	99.97	37.77	787
El Paso, TX	BW	17.6	22	106.40	31.80	1194
Ely, NV	BS	7.0	25	114.85	39.28	1906
Eugene, OR	Cs	11.2	125	123.22	44.12	109
Fresno, CA	BS	17.2	27	119.72	36.77	100
Grand Junction, CO	BS	11.4	22	108.53	39.12	1475
Great Falls, MT	Df	7.3	38	111.37	47.48	1116
Lake Charles, LA	Cf	19.5	139	93.22	30.12	3
Lander, WY	Df	6.9	33	108.73	42.82	1696
Las Vegas, NV	BW	19.4	10	115.17	36.08	664
Los Angeles, CA	BS	16.7	31	118.40	33.93	32
Madison, WI	Df	7.8	78	89.33	43.13	262
Medford, OR	Cs	11.7	48	122.87	42.37	396
Miami, FL	Aw	24.2	142	80.27	25.80	2
Midland, TX	BS	17.0	38	102.20	31.93	871
Montgomery, AL	Cf	17.9	135	86.40	32.30	62
Nashville, TN	Cf	15.0	120	86.68	36.12	180
Omaha, NE	Df	10.5	73	96.52	41.37	404
Phoenix, AZ	BW	22.7	19	112.02	33.43	339
Pittsburgh, PA	Df	10.2	93	80.22	40.50	373
Portland, OR	Cs	11.8	92	122.60	45.60	12
Raleigh, NC	Cf	14.8	104	78.78	35.87	134
Salt Lake City, UT	Cf	11.1	41	111.97	40.77	1288
Santa Maria, CA	Cs	13.5	31	120.45	34.90	72
Savannah, GA	Cf	18.6	124	81.20	32.13	16
Seattle, WA	Cs	10.9	93	122.30	47.45	122
Tallahassee, FL	Cf	19.1	166	84.37	30.38	21

[a]From formulae in Koeppe and De Long (1958). Translation (number of stations in parentheses): Df (9) – cold winter, all months moist; Cf (14) – mild winter, all months moist; Cs (5) – mild winter, dry summer; Cw (1) – mild dry winter; Aw (1) – hot wet summer, dry winter; BS (7) – hot, semiarid; BW (3) – hot, arid.

2.2. Parameterization strategy

The expression proposed by B&C for predicting R_{gh} uses a modeled estimate of daily total extraterrestrial insolation on a horizontal surface (daily total potential radiation, R_{pot}, MJ m^{-2} day^{-1}) which is reduced by a linear scalar, the daily total transmittance (T_t, unitless)

$$R_{gh} = T_t \cdot R_{pot} \quad (1)$$

where T_t is estimated as a function of the diurnal range

in air temperature ($\Delta T = T_{max} - T_{min}$, °C)

$$T_t = T_{t,max}\ 1 - \exp\ -B \cdot \Delta T^C \big) \quad (2)$$

$T_{t,max}$ (denoted A in M1), B, and C are empirical coefficients. B&C included a 2-day averaging for T_{min} in their original formulation for ΔT in M1, but we found better results without averaging. We assume that methods to estimate R_{pot} are well-developed (Garnier and Ohmura, 1968; Swift, 1976; Gates, 1980), and focus our efforts on developing methods to estimate $T_{t,max}$, B, and C.

The parameter $T_{t,max}$ in Eq. (2) is the asymptote of T_t with increasing ΔT, and represents the potential total transmittance on a given day (cloudless conditions). In M1, this parameter is assumed constant in time, but was assigned different values for each of the three stations tested (0.70, 0.77, and 0.72, for Pullman, WA, Great Falls, MT, and Seattle/Tacoma, WA, respectively). M1 includes an explicit and objective parameterization for B that makes it an exponentially decaying function of the monthly average ΔT, and assigns the parameter C a constant value of 2.4.

Here we first consider the spatial and temporal variation in daily total transmittance, in order to define an objective and physically meaningful parameterization for $T_{t,max}$. We next consider the relationship between ΔT and the daily total transmittance expressed as a fraction of $T_{t,max}$, in order to develop an objective parameterization for B and C. We then describe objective methods for estimating the resulting model's prediction accuracy and its final parameter values.

2.3. Parameterization of $T_{t,max}$

B&C note that $T_{t,max}$ will vary with site elevation, due to changes in the total atmospheric mass along the beam path from the top of the atmosphere to the surface. Ignoring changes in surface pressure due to moving air masses, the variation with elevation can be considered as constant in time for a given site and can be represented by the expression

$$\tau_z = \tau_0^{P_z/P_0} \quad (3)$$

where τ_z (unitless) is the instantaneous transmittance corrected for elevation z, τ_0 (unitless) is the instantaneous transmittance at a reference elevation, P_z is the surface air pressure at a station with elevation z, and P_0 is the surface air pressure at the reference elevation (Gates, 1980).

Through this same mechanism of varying optical thickness, instantaneous transmittance can also be described as a function of solar zenith angle (θ), which varies on average by latitude, but also at any latitude by day of year, and, for a given latitude and day of year, by solar time (Gates, 1980). Variations in instantaneous transmittance due to θ (τ_θ, unitless) can be expressed as

$$\tau_\theta = \tau_{nadir}^{m_\theta} \quad (4)$$

where τ_{nadir} (unitless) is the instantaneous cloudless-sky transmittance at solar nadir ($\theta = 0$, sun directly overhead), and m_θ (unitless) is the optical air mass for a given θ, defined as $m_\theta = 1/\cos(\theta)$, with corrections for $\theta > 70°$, according to Gates (1980).

B&C also note that atmospheric water vapor has a strong influence on transmittance. In preliminary assessments of the SAMSON database we observed an apparent influence of surface water vapor pressure on the seasonal variation in $T_{t,max}$. A strong ordinal relationship was apparent, with the highest observed transmittances through the period of record for any given yearday corresponding to relatively low water vapor pressures. We propose the following simple linear expression to account for this observation

$$\tau_{wet} = \tau_{dry} + \alpha e \quad (5)$$

where τ_{wet} is the instantaneous transmittance corrected for the influence of water vapor (unitless), τ_{dry} is the instantaneous transmittance for a dry atmosphere (unitless), e is the near-surface water vapor pressure (Pa), and α is a slope parameter (Pa^{-1}) describing the influence of e on τ.

Eqs. (3)–(5) can be combined in several different ways to give an expression for the joint influence of elevation, θ, and e on the instantaneous transmittance. After some preliminary testing we chose the following formulation for the combined effects

$$\tau_{z,\theta,wet} = \tau_{0,nadir,dry}\big)^{(P_z/P_0)\cdot m_\theta} + \alpha e \quad (6)$$

where $\tau_{z,\theta,wet}$ (unitless) is the instantaneous transmittance at elevation z, zenith angle θ, for a wet atmosphere, and $\tau_{0,nadir,dry}$ is the instantaneous transmittance (unitless) at the reference elevation, at nadir, for a dry atmosphere.

Eqs. (3)–(6) consider instantaneous transmittances under clear-sky conditions, but M1 is concerned with daily total transmittances. For a discrete-time numerical method, and assuming that the vapor pressure (e) is constant through the day, the daily total transmittance for clear-sky conditions can be related to the instantaneous clear-sky transmittance from Eq. (6) by the expression

$$T_{\mathrm{t,max}} = \left[\frac{\sum_{s=\mathrm{sr}}^{\mathrm{ss}} R_{\mathrm{pot},s} \cdot \tau_{0,\mathrm{nadir,dry}}^{(P_z/P_0)\cdot m_\theta}}{\sum_{s=\mathrm{sr}}^{\mathrm{ss}} R_{\mathrm{pot},s}}\right] + \alpha e \qquad (7)$$

where $R_{\mathrm{pot},s}$ is the instantaneous potential radiation at solar time s, and sr and ss are the times of sunrise and sunset, respectively. Eq. (7) represents a hypothesized basis for estimating a subset of the observed values of T_t: those occurring under clear-sky conditions.

To test this hypothesis, we extracted a subset of observations intended to represent, for each station, the seasonal course of the highest observed values of T_t. For each station, we took the highest observed values of T_t over the station's period of record for a given yearday to represent the highest possible T_t at that location on that yearday. This interpretation assumes that there are enough years of record to obtain a sample of T_t values at each yearday that includes at least one cloudless day. To make this analysis less sensitive to measurement error, we used a 7-day window centered on the day in question, and determined $T_{\mathrm{t,max}}$ for that station-yearday by averaging the three highest values of T_t with yeardays within the window. These values of $T_{\mathrm{t,max}}$ are referred to below as *observed* values, although we recognize that other methods of analysis could result in different values. $T_{\mathrm{t,max}}$ was assigned as missing for any station-day with less than ten observations within the 7-day window. The application of Eq. (7) requires observations of e, which we calculated from observations of T_{dew}. Values of T_{dew} corresponding to each observed $T_{\mathrm{t,max}}$ were derived by taking the three values of daily average T_{dew} associated with the selected values of T_t, and averaging to get a single value for each yearday.

These methods are illustrated in Fig. 1. Top panels show standard values of R_{pot} and observed values of R_{gh}, plotted by day of year for two stations with different climates. Temporal and spatial variation in observed transmittance is more obvious in the middle panels, where R_{gh} is transformed to T_t via Eq. (1). The value of e corresponding to the observed value of $T_{\mathrm{t,max}}$ is usually among the lowest values of e for that yearday (bottom panels).

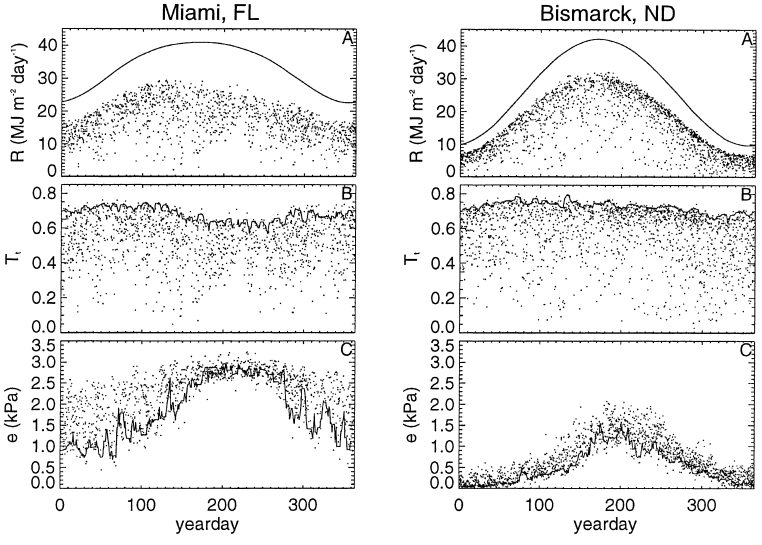

Fig. 1. Sample observations of daily radiation, transmittance, and vapor pressure (1961–1990), plotted against yearday, for two stations with contrasting climates. A: points show observed R_{gh}, solid line shows R_{pot}. B: points show observed T_t, solid line shows $T_{\mathrm{t,max}}$. C: points show vapor pressure, solid line shows vapor pressure values associated with values of $T_{\mathrm{t,max}}$ in B.

Assuming that P_z, P_0, e, and the relationship between θ and s are known, two parameters from Eq. (7) remain to be estimated; $\tau_{0,\mathrm{nadir,dry}}$ and α. We used numerical methods to find parameter values that minimized the mean absolute error (MAE) between predicted and observed values of $T_{\mathrm{t,max}}$. (P_z/P_0) was estimated for a standard atmosphere (Irbane and Godson, 1981). T_{dew} observations were used to calculate e following Abbott and Tabony (1985). Standard geometric expressions were used to estimate θ as a function of latitude, day of year, and solar time (e.g. Hungerford et al., 1989).

To test the effectiveness of Eq. (7) we carried out a series of increasingly detailed parameterizations for $T_{\mathrm{t,max}}$, comparing results for significant differences in prediction error. First, we took the value of $T_{\mathrm{t,max}}$ to be constant in space and time (CST), and set it as the observed average of $T_{\mathrm{t,max}}$ over all stations for all yeardays. Second, we took the value for $T_{\mathrm{t,max}}$ to be constant in time (CT) for each station, and set it as the observed average of $T_{\mathrm{t,max}}$ for the station. Third, we took $T_{\mathrm{t,max}}$ to be constant in space (CS) on any given yearday, and set it as the observed average of $T_{\mathrm{t,max}}$ over all stations for that yearday. For these three tests a numerical parameter selection process was not necessary. Next, we tested the three separate components of Eq. (7) independently. These three tests are referred to below as (z), (θ), and (e). The three possible combinations of these three components taken two at a time were tested next, using the ordering logic implicit in Eq. (7). These three tests are referred to below as (z,θ), (z,e), and (θ,e). The final test was for all three components taken together, as in Eq. (7).

Paired t-tests were performed on the absolute errors for each station-day ($n = 12205$) between pairs of methods. Methods with no significant difference in MAE ($p > 0.005$) were ranked together. The parameterization approach used for estimating $T_{\mathrm{t,max}}$ in the rest of the study was determined by choosing the approach with the lowest-ranking MAE, choosing the simpler approach in the case of equal rankings.

2.4. Parameterization of B and C

We followed the logic of M1 in developing a more general method for estimating B and C. One significant departure of our analysis from M1 is due to the spatial and temporal variability of $T_{\mathrm{t,max}}$. In M1, T_{t} on each day is predicted as a function of ΔT, but here, instead of T_{t}, we predict the realized proportion of $T_{\mathrm{t,max}}$ as a function of ΔT, calling this proportion $T_{\mathrm{f,max}}$:

$$T_{\mathrm{f,max}} = \frac{T_{\mathrm{t}}}{T_{\mathrm{t,max}}} \tag{8}$$

Another departure from M1 is that we have defined a minimum value for $T_{\mathrm{f,max}}$. We set this minimum value to 0.1 by examining values of $T_{\mathrm{f,max}}$ determined from Eq. (8) using observed T_{t} from the SAMSON database and predicted $T_{\mathrm{t,max}}$ from the previous section. Given these changes, the revised expression involving the B and C parameters is

$$T_{\mathrm{f,max}} = 1.0 - 0.9 \cdot \exp\left(-B \cdot \Delta T^{C}\right) \tag{9}$$

M1 includes a correction for wet days, and after testing a number of different possibilities, we arrived at a similar correction. On days with precipitation, the value of $T_{\mathrm{f,max}}$ predicted from Eq. (9) was multiplied by a constant factor to obtain the corrected prediction. This correction in M1 was applied to observations of ΔT, but we found that better results were obtained by applying the correction to $T_{\mathrm{f,max}}$. We tested a range of multipliers, and found the best results with the multiplier set to 0.75. After this correction is applied to $T_{\mathrm{f,max}}$, the final expression for estimated R_{gh} is

$$R_{\mathrm{gh}} = R_{\mathrm{pot}} \cdot T_{\mathrm{t,max}} \cdot T_{\mathrm{f,max}} \tag{10}$$

In the original parameterization of M1 it was shown that optimal values for B follow an exponentially decreasing function of the monthly average value of ΔT. We explored several alternative parameterizations, and found that this same basic parameterization strategy applies to Eq. (9) and to the extended range of climates represented in the SAMSON database. For each station-day we calculated the average of ΔT for that day and the previous 29 days ($\overline{\Delta T}$), correcting for cases of missing temperature data. Grouping together the observations from all stations and sorting by R_{pot} and $\overline{\Delta T}$, we divided the observations into equal-sized subsets. Taking each subset individually, we performed a numerical optimization for B by selecting a value that minimized the MAE for predictions of R_{gh} from Eq. (10), comparing against the daily observations of R_{gh} from the SAMSON database. An exponential curve was fit to the set of points consisting of the optimal values for B and the associated subset

means of $\overline{\Delta T}$, using an automated numerical curve-fitting procedure that minimized prediction error for B. We found that the following three-parameter exponential decay curve, including a y-axis offset parameter (b_0), was more appropriate than the two-parameter function used in M1

$$B = b_0 + b_1 \cdot \exp(-b_2 \cdot \overline{\Delta T}) \quad (11)$$

The resulting empirical expression for the prediction of B was then applied to the values of $\overline{\Delta T}$ from the entire dataset, followed by predictions of R_{gh} from Eqs. (9) and (10), to generate an overall MAE. This process of numerical optimization, curve fitting, and reassessment of MAE was carried out over a range of values for C to find the value which, when held constant over space and time (as in M1), resulted in the lowest overall MAE.

2.5. Cross-validation analysis

We used cross-validation to estimate bias and error in the final model predictions of $T_{t,max}$ and R_{gh}. The ability to objectively define model parameters is a prerequisite for an analysis of model bias and error using cross-validation (Efron, 1983; Efron and Tibshirani, 1997). Given the somewhat subjective development of model *structure* described in the previous two sections, *parameter values* for the resulting model were objectively determined by searching in discrete steps through prescribed regions of the parameter space to find a local minimum MAE. The cross-validation analysis proceeded by: (1) dropping one station at a time out of the database; (2) using the data from the remaining stations to objectively determine a set of model parameters; (3) applying the resulting model to predict $T_{t,max}$ and R_{gh} for the withheld station; (4) comparing those predictions with the observed values to determine MAE and bias for the withheld station; and (5) repeating from step (1), returning the withheld station to the database and dropping out a single other station, until all stations had been withheld once.

Step (2) in this process consisted of a multi-way test of parameter ranges that optimized parameter values by minimizing pooled MAE across all observations except those at the dropped station. The parameters $\tau_{0,nadir,dry}$ and α were selected on the basis of minimized MAE for predictions of $T_{t,max}$, according to Eq. (7). Given these parameters, values for C and for the coefficients of Eq. (11) were selected to minimize MAE for predictions of R_{gh}.

2.6. Final model formulation

We applied the objective parameterization procedure just described for the entire set of observations (all stations included) to produce the final model parameters.

3. Results and discussion

3.1. Parameterization of $T_{t,max}$

The (z,θ,e) method, Eq. (7), had the lowest MAE, significantly lower than any of the other simpler methods tested (Table 2). The CT method is essentially the same logic employed by B&C for specifying $T_{t,max}$, and it ranked third in these tests. The (z,θ,e) method represents a reduction in error of 28% from the original M1 method, and a 44% reduction in error from the CST method, employed in an early application of M1 by Running et al. (1987). In addition to providing better predictions, Eq. (7) has the great advantage over these previous methods of not requiring any radiation observations (or assumptions about radiation conditions) at a new site. The physical basis of the two required parameters suggests that their optimal values should be largely independent of geographical location.

Most seasonal and geographic components of variation in $T_{t,max}$ are captured by Eq. (7), but some

Table 2
Comparison of various methods for predicting $T_{t,max}$

Method	MAE	Bias	τ	α (Pa^{-1})	Rank
CST	0.0398	–	–	–	7
CT	0.0307	–	–	–	3
CS	0.0339	–	–	–	4
(z)	0.0351	+0.0074	0.705	–	5
(θ)	0.0452	+0.0092	0.850	–	9
(e)	0.0370	+0.0098	0.745	$-2.75e-5$	6
(z,θ)	0.0412	+0.0070	0.840	–	8
(z,e)	0.0343	+0.0092	0.720	$-1.50e-5$	4
(θ,e)	0.0231	+0.0014	0.880	$-6.75e-5$	2
(z,θ,e)	0.0222	+0.0021	0.870	$-6.10e-5$	1

Table 3
Results of cross-validation analysis for predictions of $T_{t,max}$ and R_{gh}

Station	Predictions of $T_{t,max}$			Predictions of R_{gh}				
	n	MAE (Unitless)	Bias (Unitless)	n	MAE (MJ m^{-2} day^{-1})	Bias (MJ m^{-2} day^{-1})	MAE (% of observed)	Bias (% of observed)
Albany, NY	84	0.041	0.020	312	3.31	2.48	35.4	26.5
Albuquerque, NM	359	0.017	−0.005	2825	1.95	−0.36	9.6	−1.8
Bismarck, ND	359	0.037	−0.027	1633	2.19	0.80	14.8	5.4
Boise, ID	359	0.021	0.006	1509	2.00	1.06	12.4	6.6
Boston, MA	2	0.016	−0.016	167	2.05	−1.13	12.2	−6.8
Boulder, CO	359	0.032	0.030	2401	3.09	2.30	19.7	14.7
Brownsville, TX	359	0.024	−0.012	1802	2.89	0.35	17.2	2.1
Burlington, VT	333	0.031	0.023	985	2.68	1.63	19.6	11.9
Cape Hatteras, NC	16	0.018	−0.013	208	3.49	−3.24	18.1	−16.8
Caribou, ME	234	0.047	0.015	557	2.78	1.73	22.2	13.8
Charleston, SC	164	0.015	−0.010	458	1.64	−0.93	8.6	−4.9
Columbia, MO	359	0.019	−0.015	740	2.48	0.80	14.9	4.8
Daytona Beach, FL	359	0.020	−0.011	1107	3.11	−1.59	17.2	−8.8
Dodge City, KS	359	0.017	−0.015	1208	1.95	−0.57	10.0	−2.9
El Paso, TX	359	0.014	−0.002	2462	2.05	−1.09	9.5	−5.1
Ely, NV	350	0.021	0.007	1313	2.34	1.33	13.8	7.8
Eugene, OR	359	0.019	0.018	3209	2.98	2.65	23.4	20.8
Fresno, CA	359	0.018	−0.014	2084	1.59	−0.39	7.5	−1.9
Grand Junction, CO	235	0.026	0.018	604	2.10	0.61	11.8	3.4
Great Falls, MT	358	0.025	−0.008	1263	2.21	1.00	15.2	6.9
Lake Charles, LA	319	0.023	−0.019	769	2.39	−0.48	13.2	−2.6
Lander, WY	356	0.022	0.011	1429	2.45	1.17	14.4	6.9
Las Vegas, NV	359	0.010	0.002	1626	1.94	−0.45	9.1	−2.1
Los Angeles, CA	319	0.021	0.011	770	3.11	−2.16	17.1	−11.9
Madison, WI	356	0.028	−0.001	1314	2.66	1.56	20.7	12.1
Medford, OR	359	0.017	−0.001	1848	1.88	0.90	10.7	5.1
Miami, FL	358	0.016	−0.005	1248	3.93	−2.70	22.9	−15.7
Midland, TX	312	0.010	0.005	774	2.16	−0.60	10.8	−3.0
Montgomery, AL	359	0.018	0.014	1299	2.31	0.81	13.6	4.7
Nashville, TN	359	0.017	−0.013	1721	2.05	0.47	11.8	2.7
Omaha, NE	359	0.024	−0.016	1475	2.38	0.62	14.7	3.8
Phoenix, AZ	359	0.022	−0.019	2556	1.99	−1.19	9.7	−5.8
Pittsburgh, PA	141	0.043	0.042	425	2.90	2.11	21.4	15.6
Portland, OR	359	0.037	0.032	1301	2.86	2.54	24.9	22.0
Raleigh, NC	319	0.027	0.027	714	2.38	1.11	14.4	6.7
Salt Lake City, UT	359	0.034	0.034	1666	2.33	1.11	14.2	6.8
Santa Maria, CA	65	0.018	−0.013	283	1.53	−0.91	8.0	−4.8
Savannah, GA	359	0.015	−0.012	1505	2.36	−0.05	14.2	−0.3
Seattle, WA	359	0.021	0.005	1657	2.54	2.14	21.9	18.5
Tallahassee, FL	345	0.017	0.012	1243	2.33	1.20	15.2	7.8
All stations	12205	0.023	0.002	52470	2.39	0.51	14.9	4.3

problems are apparent (Table 3, Fig. 2). Several stations have a strong positive prediction bias through most of the year (Salt Lake City and Boulder, among others). High aerosol concentrations may be responsible for these offsets: both Salt Lake City and Boulder are known to have significant air pollution problems, due to topographic settings that result in local inversions. In addition to urban pollution, salt aerosols, dust storms, and smoke from seasonal burning and wildfire are also likely to have an influence on transmittance at various locations and times through the year. Another possibility is that topographic elements block direct

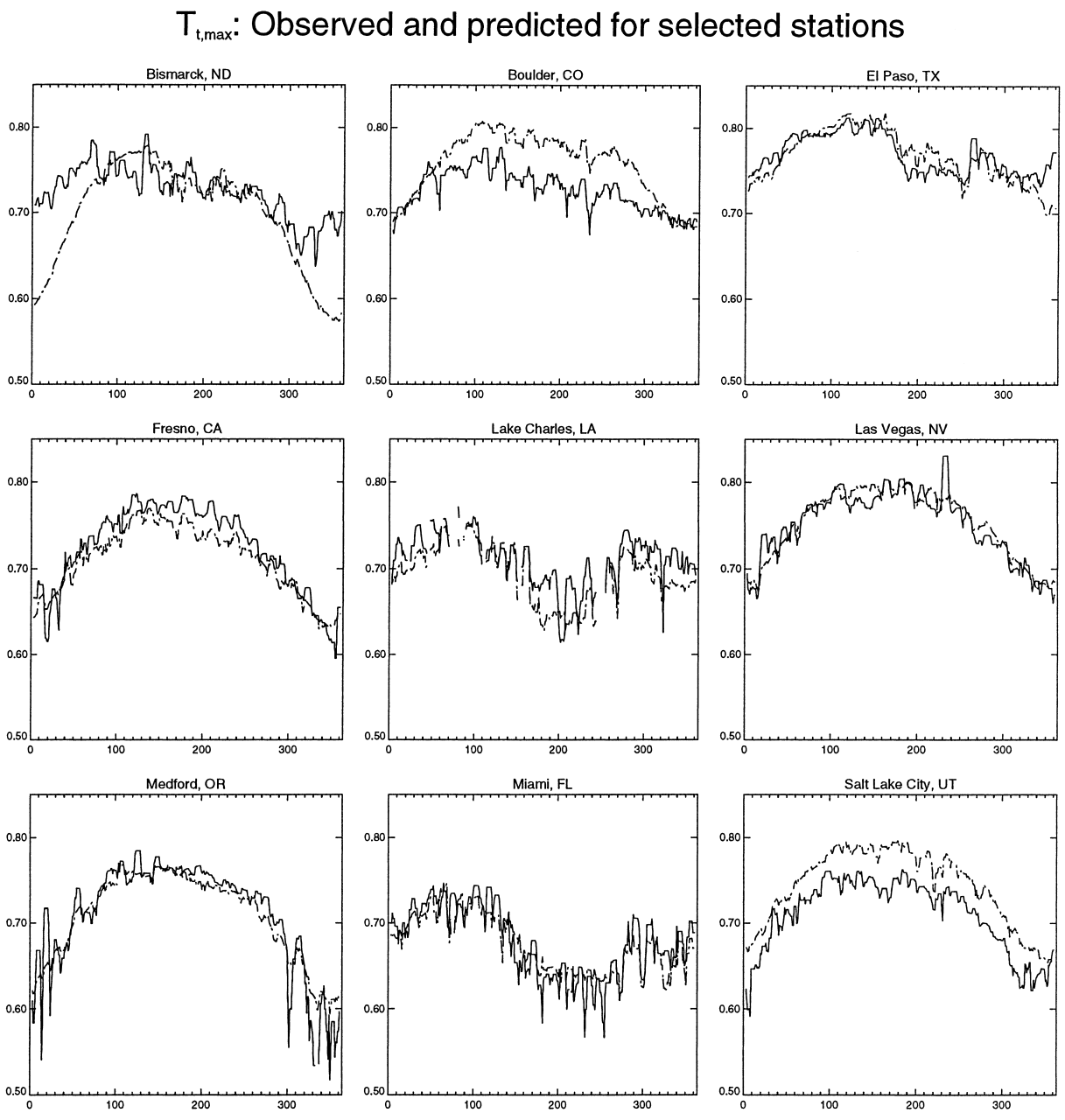

Fig. 2. Observed (solid) and predicted (dashed) $T_{t,max}$ at nine stations with relatively complete annual records. Predictions use the (z,θ,e) model. For each plot, x-axis is yearday and y-axis is $T_{t,max}$ (unitless). Stations are arranged alphabeticaly.

sunlight at the observation locations during some parts of the day. This variation would result in positive prediction biases, since the algorithm used here to predict potential radiation assumes that the horizons are unobstructed at all times. These problems might be resolved through a more detailed analysis of the hourly radiation observations, and with the help of site-specific aerosol data. Measurement error and instrumentation differences could also explain some biases.

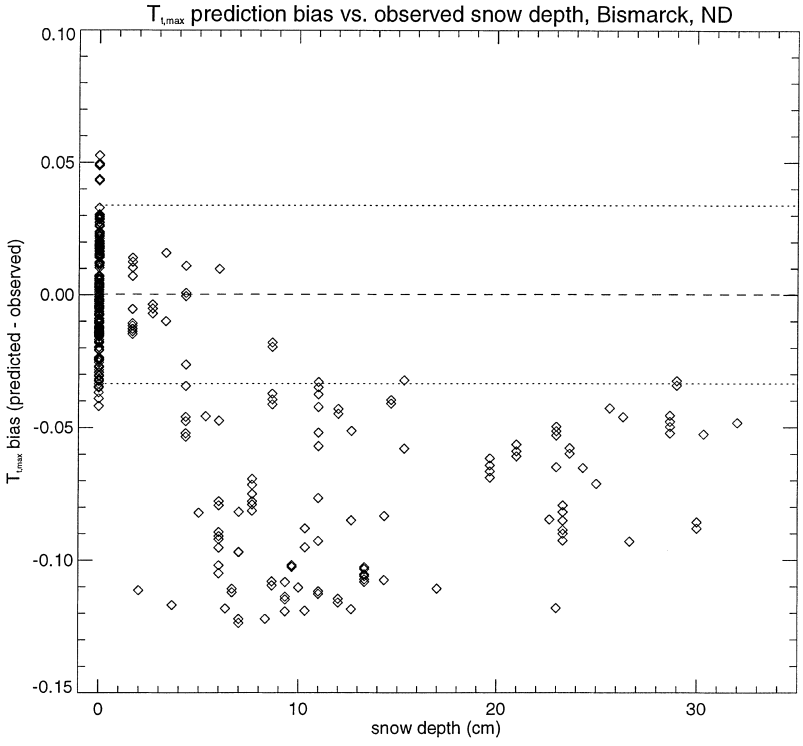

Fig. 3. Influence of snowdepth on bias in $T_{t,max}$ predictions, at Bismarck, ND. Dashed line is the mean bias for days without snow, dotted lines show ± two standard deviations for this mean.

Another apparent problem is a negative prediction bias during the winter for some of the coldest stations (e.g., Madison, WI, Great Falls, MT, and Bismarck, ND). A possible explanation for these underpredictions is that snow-covered ground results in higher observed daily transmittance than would otherwise be expected, due to multiple reflections between the surface and the atmosphere (Kiehl, 1992). We used observations of snow depth from the SAMSON database to explore this possibility, and found a correspondence between snow depth and the prediction bias for $T_{t,max}$. Fig. 3 shows an example of this correspondence for Bismarck, ND, where the prediction bias for most days with snow on the ground was usually negative and well outside the range of biases observed on days without snow. The multiple reflection effect is related more to fractional snow cover in the region around the station than to snow depth at the station. At Bismarck, bias is negative but shows little pattern with increasing snow depths above 10 cm. There should, however, be a positive relationship between snow depth and fractional coverage for the surrounding area in the lower range of snow depth, due to spatial variation in snow accumulation and melting (Sellers, 1992). Such a relationship can be inferred from Fig. 3, in the range of snow depth from 0 to 10 cm. In that range bias values for the lowest snow depths are similar to those observed under snowless conditions, with a general trend towards increasing negative bias with increasing snow depth.

It seems likely, from this crude analysis, that some kind of snow-cover component in the model would lead to improved predictions of $T_{t,max}$ in snowy climates. In the absence of observed fractional snow cover for sites where the solar radiation model is to be applied, a snow accumulation and melt component of some sort would need to be added to the model. Plenty of candidate snow-models exist, but their application to the M1 algorithm is beyond the scope of this study. We note that the same multiple reflection effect should apply to other high-albedo cases, such as for bright soils with low vegetation cover.

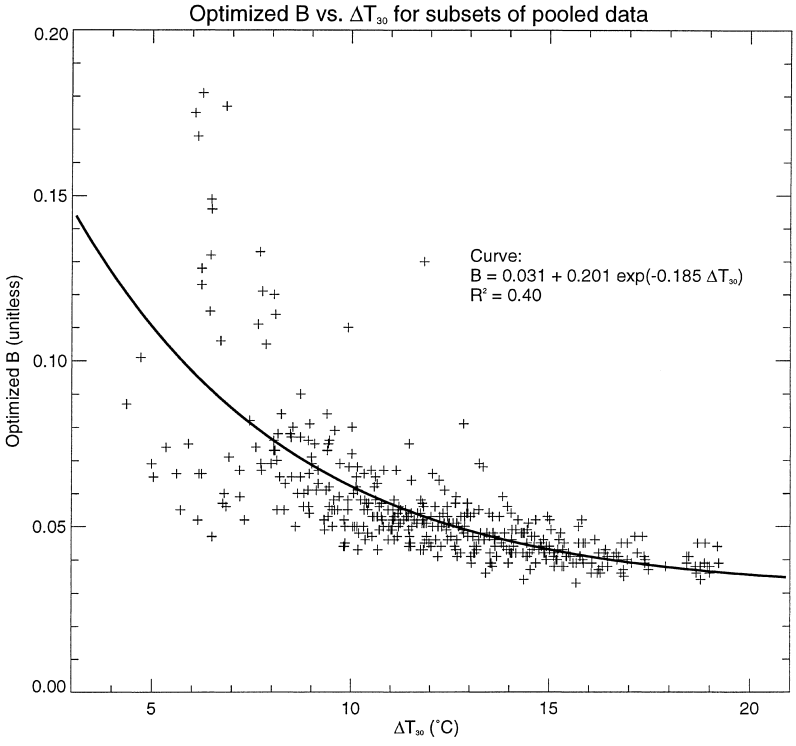

Fig. 4. Fitted parameters for Eq. (11) derived from optimized values for B over 400 sorted subsets ($n = 133$ station-days per subset) of daily data.

3.2. Parameterization of B and C

Fig. 4 shows an example of the optimized values of B for each of 400 ordered subsets of daily data ($n = 133$ station-days per subset), plotted against the subset means of $\overline{\Delta T}$. The solid line shows Eq. (11) fit to these data ($R^2 = 0.40$). These optimized values for B were determined with $\tau_{0,\mathrm{nadir,dry}} = 0.87$, $\alpha = -6.1e-5$, and $C = 1.5$. We found that Eq. (11) fits the optimized values of B equally well over a range of values for C, although the values for b_0, b_1, and b_2 vary significantly with changes in C.

B&C noted that their empirical expression for predicting B was derived for stations receiving most of their precipitation in the winter, and that stations with a summer maximum might follow a different pattern. The SAMSON database includes both winter- and summer-maximum precipitation stations, as well as intermediate cases. When optimal values of B were determined for ordered subsets of $\overline{\Delta T}$ from individual stations, we found that the relationship between optimized values of B and $\overline{\Delta T}$ varied across the winter–summer precipitation gradient (Fig. 5). By pooling data from all stations, our method results in predictions for B from Eq. (11) that are too high for the winter-precipitation stations and too low for the summer-precipitation stations (Fig. 5, inset). These biases are most severe for the lower range of $\overline{\Delta T}$ (overcast periods). Overestimates (underestimates) of B result in overestimates (underestimates) of $T_{\mathrm{f,max}}$ and R_{gh}.

It seems plausible that the trend of decreasing B with increasing $\overline{\Delta T}$ (observed to varying degrees for all stations in this study) is related to surface energy partitioning, with a given observed value of ΔT requiring more energy input for a wet surface than for a dry one. This physical relationship is obscured in our analysis, as well as in M1, by the fact that we are relating a proportional index of R_{gh} ($T_{\mathrm{f,max}}$) to ΔT, instead of predicting R_{gh} directly. So, while a given ΔT and surface moisture state may indicate a unique R_{gh}, the physical relationship does not indicate a unique value of T_{t}, or $T_{\mathrm{f,max}}$, since these are related

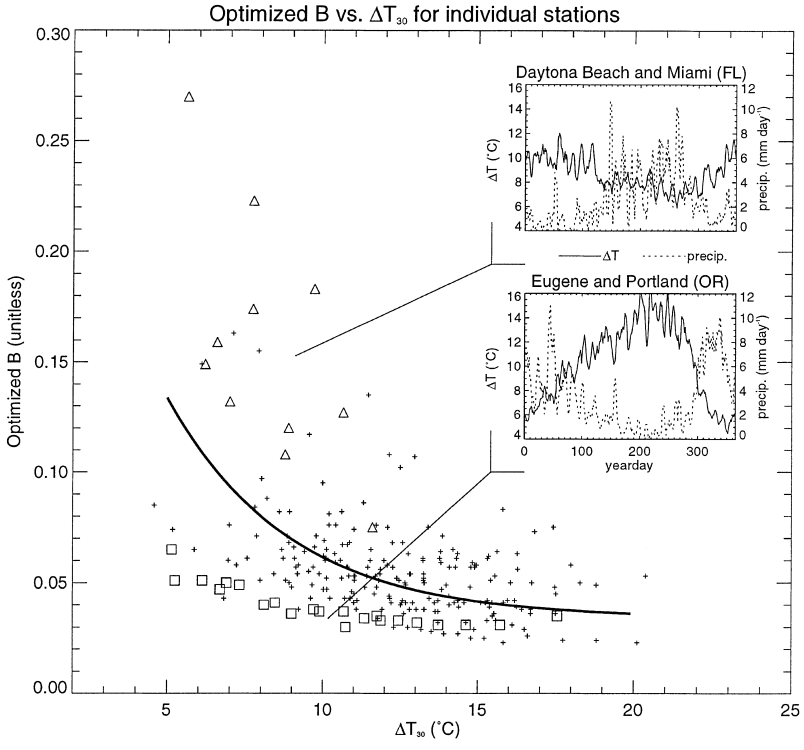

Fig. 5. Curve from Fig. 4 overlaid on optimized values of B derived from sorted subsets of daily data taken from individual stations. Square symbols are from data at Eugene and Portland, triangle symbols are from data at Daytona Beach and Miami. Inset graphs illustrate the contrast in seasonal patterns of precipitation and ΔT between these two subsets of stations.

to R_{gh} through R_{pot}, which is varying. Another potentially confounding factor is the depth of the well-mixed layer of air near the surface, which will vary with radiation input and near-surface atmospheric stability. The mixed-layer depth during the period of low $\overline{\Delta T}$ will typically be greater for summer- than for winter-precipitation stations, so a given daily ΔT in the summer-precipitation case requires more energy input, having changed the temperature of a larger volume of air. We tried various alternative forms for Eq. (11) in an attempt to account for these influences, but we found no single variable or combination of variables that gave better final estimates of R_{gh} than the form shown here. Alternative forms which improved predictions for the extreme stations, such as the inclusion of R_{pot} as a predictor, resulted in poorer predictions for the intermediate stations and an overall reduction in prediction accuracy.

Despite the low R^2 for the curve in Fig. 4, and the apparently poor behavior of Eq. (11) at the extremes of the winter- versus summer-precipitation gradient (Fig. 5), we found that predictions of R_{gh} using Eq. (11) were degraded by only 10% compared to predictions of R_{gh} using the optimized values of B shown in Fig. 4 (MAE from Eq. (11) of 2.3 MJ m^{-2} day^{-1}, versus 2.1 MJ m^{-2} day^{-1} when using the optimal values of B). It may be that by accurately describing the spatial and temporal variation in $T_{t,max}$, our method avoids larger errors from an inadequate parameterization of B.

3.3. Cross-validation

Table 3 shows the cross-validation MAE and bias for predictions of $T_{t,max}$ at each station. After weighting for the number of observations at each station, the pooled MAE is 0.0224 (about 3.2% of the observed pooled mean value for $T_{t,max}$) and the pooled bias is +0.0016 (about +0.2% of observed $T_{t,max}$). For all stations, the optimal value for $\tau_{0,nadir,dry}$ was 0.87, and

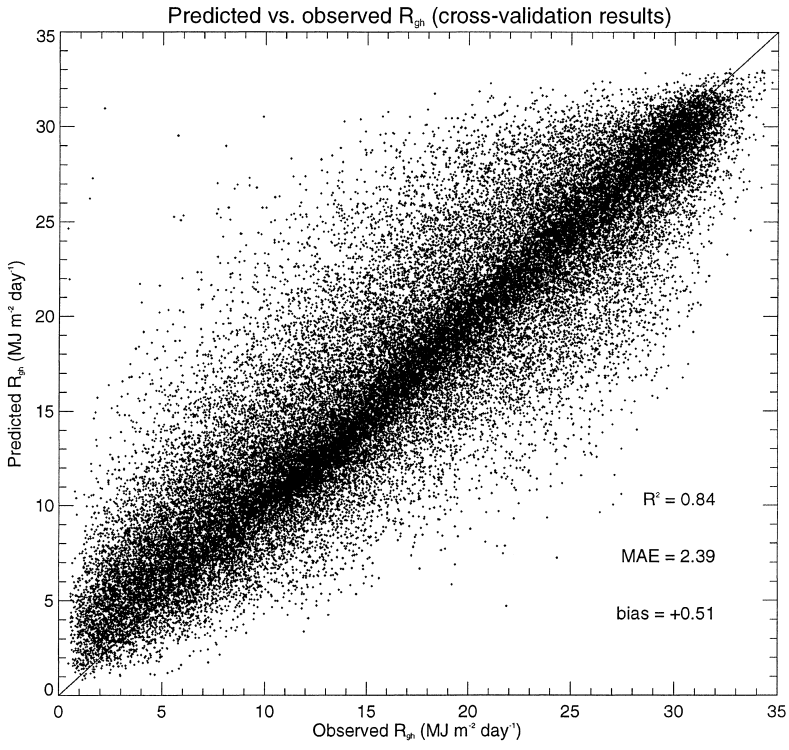

Fig. 6. Cross-validation predictions vs. observations for R_{gh}, pooled for all stations, $n = 52470$ station-days.

the optimal value for α was either $-6.1e-5$ or $-6.2e-5$.

Cross-validation estimates of MAE and bias for prediction of R_{gh} at each station are also shown in Table 3. When weighted by the number of observations at each station, the resulting pooled MAE is 2.39 MJ m^{-2} day^{-1}, and the pooled bias is +0.51 MJ m^{-2} day^{-1}. The cross-validation optimized value of C for each station was either 1.5 or 1.4. Cross-validation values for the coefficients of Eq. (11) were more variable. To illustrate the pattern of error in the pooled dataset, daily predictions versus observations are plotted together for all stations in Fig. 6.

With a few exceptions, the highest and lowest values of observed R_{gh} are predicted very well, with reduced prediction accuracy in the middle range of the observations. Partly cloudy days are likely to fall in this middle range. We expect lower model accuracy on days with partial cloud cover than on days with complete cloud-cover or on clear days, since the model relies on the difference between two instantaneous temperatures (the daily maximum and minimum), and since partial cloud cover will induce high variance in sub-daily air temperatures. It may not be possible to overcome this source of error without abandoning the basic premise of the model.

Fig. 7 shows the temporal variation in model performance, by day of year. MAE, when measured in MJ m^{-2} day^{-1}, increases from January through March, is highest from April through August, and falls off again through December. By plotting the same errors as a percent of the mean observed values on each day, it is clear that summer errors are high due to the greater overall radiation loads, and as a percent are only half as large as the winter errors. Seasonal variation in bias shows a strong pattern, with small negative biases (underpredictions) around mid-summer and larger positive biases through the fall and winter, with a peak positive bias in the spring. Since the bias for many stations is relatively close to zero throughout the year, pooled seasonal variations are strongly influenced by a small number of stations with strong and seasonally varying biases, some possible causes of which have already been addressed.

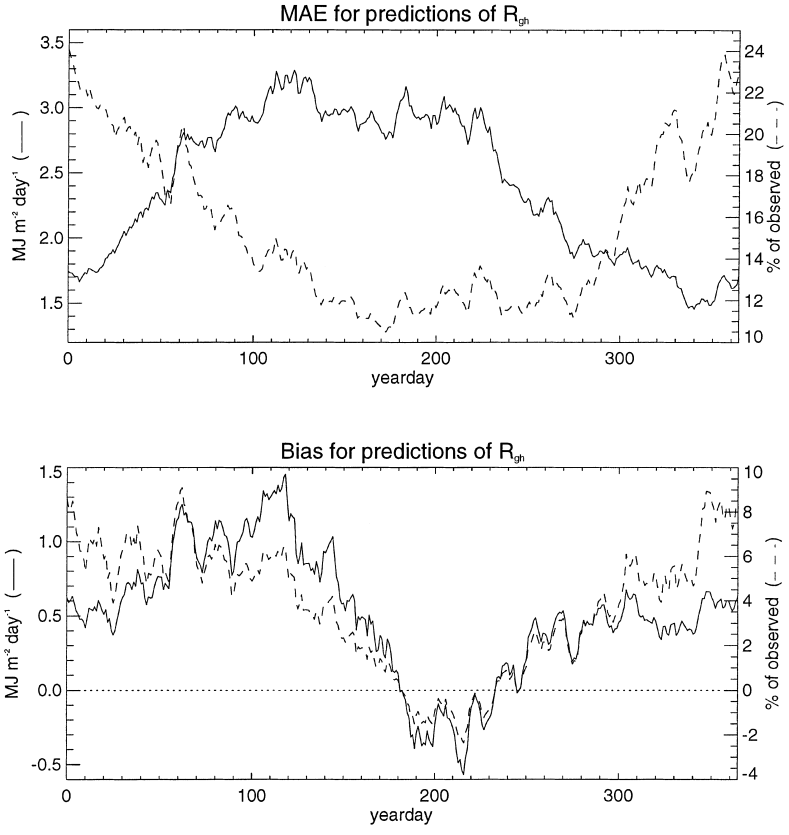

Fig. 7. Temporal variation in cross-validation MAE and bias for predictions of R_{gh}.

The cross-validation statistics by Köppen climate codes are shown in Table 4. The most obvious differences are in the biases for predictions of R_{gh}, with the highest positive value for the Cs stations, all of which are in the Pacific Northwest coastal area, and the lowest negative value for the Aw code, represented here by a single station, Miami. These extreme biases result from the inadequate predictions of B from Eq. (11). It is interesting to note that the errors for these stations (Cs and Aw) for predictions of $T_{t,max}$ are

Table 4
Cross-validation results by Köppen codes

Code (stations)	Predictions of $T_{t,max}$			Predictions of R_{gh}				
	n	MAE (Unitless)	Bias (Unitless)	n	MAE (MJ m^{-2} day^{-1})	Bias (MJ m^{-2} day^{-1})	MAE (% of observed)	Bias (% of observed)
Df (9)	2580	0.031	0.002	9393	2.48	1.22	17.5	8.9
Cf (14)	4037	0.021	0.002	15206	2.45	0.52	14.6	3.5
Cs (5)	1501	0.023	0.012	8298	2.58	2.02	19.9	16.2
Cw (1)	359	0.024	−0.012	1802	2.89	0.35	17.2	2.1
Aw (1)	358	0.016	−0.005	1248	3.93	−2.70	22.9	−15.7
BS (7)	2293	0.019	0.003	9879	2.05	−0.03	11.0	0.2
BW (5)	1077	0.015	−0.007	6644	2.00	−0.97	9.5	−4.6

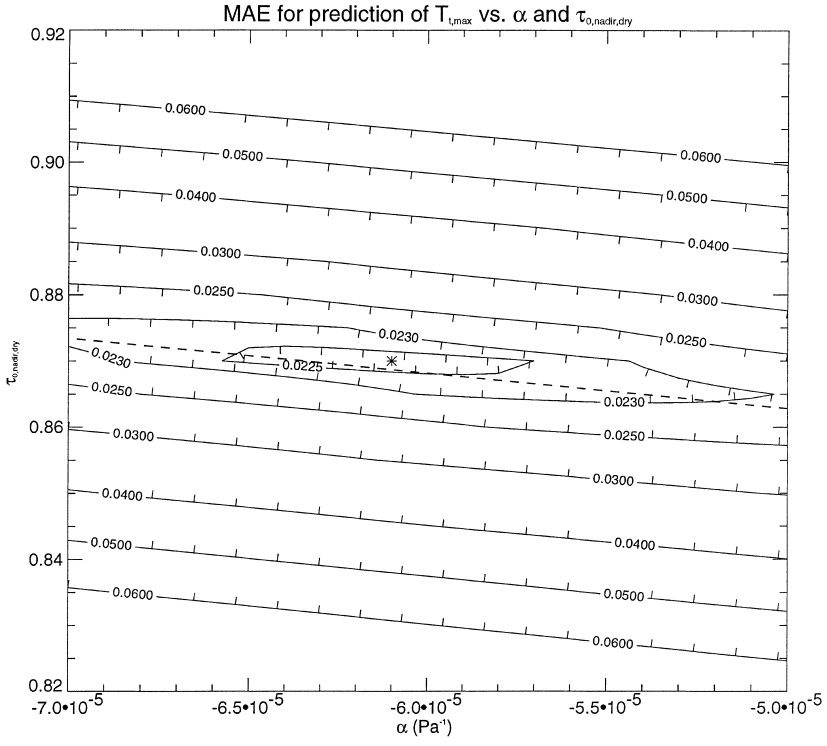

Fig. 8. Surface of MAE for predictions of $T_{\mathrm{t,max}}$, showing variation over a range of values for α and $\tau_{0,\mathrm{nadir,dry}}$. Dashed line shows the bias = 0.0 contour, and asterisk marks the parameter pair selected as the final model parameters. Tick marks on contour lines point toward lower values of MAE.

not very different from the other non-arid codes, indicating that Eq. (7) performs well in these climates. Predictions for both $T_{\mathrm{t,max}}$ and R_{gh} are better for the semi-arid and arid stations (BS and BW) than for the other climates. This result is to be expected, since clear-sky transmittance at these stations is less influenced by water vapor, and variation in R_{gh} is influenced more strongly by R_{pot} than in the wetter climates.

3.4. Final model formulation

Fig. 8 shows a contour plot of pooled MAE for predictions of $T_{\mathrm{t,max}}$ over ranges in both $\tau_{0,\mathrm{nadir,dry}}$ and α, using Eq. (7). The asterisk marks the location of the optimal parameter pair: $\tau_{0,\mathrm{nadir,dry}} = 0.870$, $\alpha = -6.1e-5$. The dashed line in Fig. 8 indicates the 0.0 contour for prediction bias, illustrating that bias and MAE are optimized at very nearly the same parameter values. Variation in pooled MAE and bias for predictions of R_{gh} over a range of values for C shows an optimal value of $C = 1.5$ (Fig. 9). The fitted coefficients for Eq. (11) with $C = 1.5$ are: $b_0 = 0.031$, $b_1 = 0.201$, and $b_2 = 0.185$.

3.5. Dewpoint temperature requirement

It was the explicit intention in the original formulation of M1 to allow predictions of R_{gh} from observations only of daily maximum and minimum temperatures and daily precipitation, since these are the variables most commonly available from current and historic surface observation networks. We have violated that logic here by assuming that dewpoint temperature observations are also available at the prediction site. For the primary stations in the SAMSON database, this assumption is valid, but in general it is not. As in our previous work in estimating daily

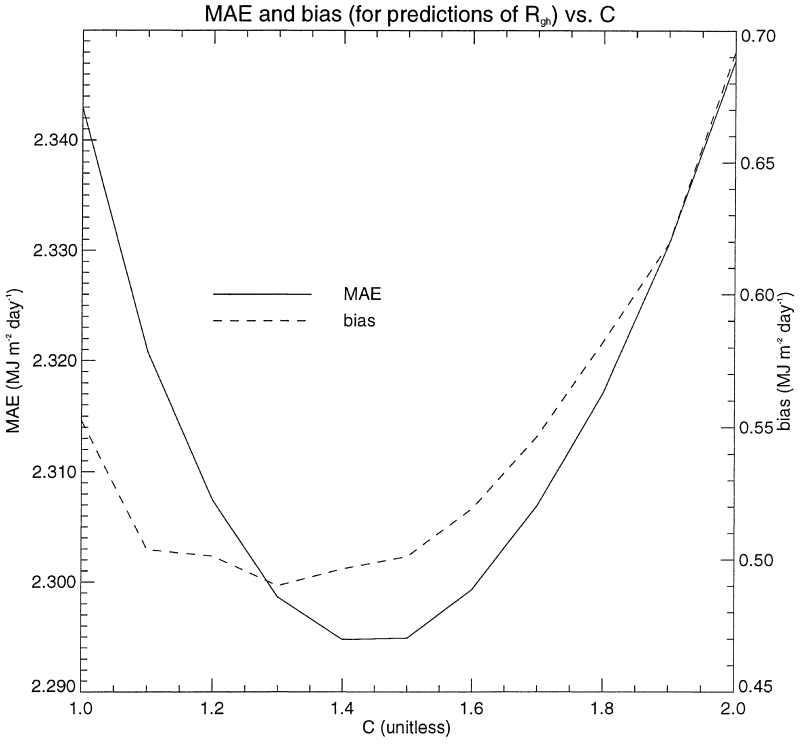

Fig. 9. Cross-validation MAE and bias for predictions of R_{gh} over a range of values for C.

surface meteorological variables (Running et al., 1987; Thornton et al., 1997), the impetus for this analysis has been to improve our ability to perform terrestrial ecosystem process simulations over spatial domains sufficiently large that installing new instrumentation is not practical. The current study will be useful in that respect only if we are able to overcome the lack of dewpoint temperature observations.

Kimball et al. (1997) presented a method for the estimation of dewpoint temperature from observations of daily air temperature and precipitation that may help us resolve this problem. Their method improves on estimates made from the assumption that dewpoint temperature and daily minimum temperature are approximately equal (Running et al., 1987), but requires an estimate of radiation as an input. In preliminary tests, we found that an iterative scheme results in predictions for both radiation and humidity that are nearly as good as those obtained from the independent algorithms driven by observations of humidity (as reported here) or radiation (as reported by Kimball et al., 1997). We are continuing to explore the union of these two methods.

3.6. Application to other climates

Although the SAMSON database covers a wide range of temperate climates, it lacks stations in tropical or boreal climates. Further model development should focus on a global distribution of observations, with an emphasis on tropical sites. Good performance at stations in the north-central U.S. suggests that our method may perform well in boreal climates, especially if the snowcover dependence (Fig. 3) can be formalized. On the other hand the fact that Miami, our only tropical station, has the largest MAE and the second-worst bias for predictions of R_{gh} suggests that some correction for tropical climates will be required. Information on seasonal precipitation patterns might be used to derive a crude atmospheric stability index to further constrain predictions of B, but tests of this notion will require more tropical data.

3.7. Application over complex terrain

Although the range in station elevations for our study is nearly 2000 m, the distribution of observations is not suited to an analysis of these methods with respect to radiation variations driven by complex terrain. This is especially true for applications in an extrapolation framework, where observations of temperature and precipitation from a station at low elevation are taken to represent the conditions at a higher elevation, after applying correction factors (as in Running et al., 1987). It is generally true in the mountainous parts of the current study area that maximum temperature decreases with elevation more rapidly than does minimum temperature (Thornton et al., 1997). Under these conditions ΔT is reduced with increasing elevation, resulting in lower predictions of R_{gh} over high terrain than over adjacent low terrain. In previous applications we have ignored the variation in temperature with elevation when estimating transmittance at a site in higher terrain than the nearest observations (Thornton et al., 1997). A more satisfying solution will require the establishment of observation networks in a number of mountainous locales, preferably with disparate climates.

Acknowledgements

Thanks to Tim Kittel, Nan Rosenbloom, Emil Cienciala, Jerry Winslow, and Steve Piper for helpful discussions, and to Michael White and two anonymous reviewers for comments on the manuscript. This research was supported in part by NASA Contracts NAGW-3151 and NAG5-6575.

References

Abbott, P.F., Tabony, R.C., 1985. The estimation of humidity parameters. Meteorol. Magazine 114, 49–56.

Bristow, K.L., Campbell, G.S., 1984. On the relationship between incoming solar radiation and daily maximum and minimum temperature. Agric. Forest Meteorol. 31, 159–166.

Efron, B., 1983. Estimating the error rate of a prediction rule: improvement on cross-validation. J. Am. Statistical Assoc. 78(382), 316–331.

Efron, B., Tibshirani, R., 1997. Improvements on cross-validation: the .632+ bootstrap method. J. Am. Statistical Assoc. 92(438), 548–560.

Garnier, B.J., Ohmura, A., 1968. A method of calculating the direct shortwave radiation income of slopes. J. Appl. Meteorol. 7(5), 796–800.

Gates, D.M., 1980. Biophysical Ecology. Springer, New York.

Glassy, J.M., Running, S.W., 1994. Validating diurnal climatology logic of the MT-CLIM model across a climatic gradient in Oregon. Ecological Applications 4(2), 248–257.

Hungerford, R.D., Nemani, R.R., Running, S.W., Coughlan, J.C., 1989. MT-CLIM: a mountain microclimate simulation model. U.S. Forest Service Research Paper, INT-414.

Hunt Jr., E.R., Piper, S.C., Nemani, R., Keeling, C.D., Otto, R.D., Running, S.W., 1996. Global net carbon exchange and intra-annual atmospheric CO_2 concentrations predicted by an ecosystem process model and three-dimensional atmospheric transport model. Global Biogeochemical Cycles 10(3), 431–456.

Irbane, J.V., Godson, W.L., 1981. Atmospheric Thermodynamics. Reidel, Dordrecht, The Netherlands.

Kiehl, J.T., 1992. Atmospheric general circulation modeling. In: Trenberth, K.E. (Ed.), Climate System Modeling. Cambridge University Press, London, pp. 319–369.

Kimball, J.S., Running, S.W., Nemani, R., 1997. An improved method for estimating surface humidity from daily minimum temperature. Agric. Forest Meteorol. 85, 87–98.

Kittel, T.G.F., Rosenbloom, N.A., Painter, T.H., Schimel, D.S., VEMAP Modelling Participants, 1995. The VEMAP integrated database for modelling United States ecosystem/vegetation sensitivity to climate change. J. Biogeography 22, 857–862.

Kittel, T.G.F., Royle, J.A., Daly, C., Rosenbloom, N.A., Gibson, W.P., Fisher, H.H., Schimel, D.S., Berliner, D.S., VEMAP2 Participants, 1997. A gridded historical (1895–1993) bioclimate dataset for the conterminous United States. 10th Conference on Applied Climatology, Reno, NV. American Meteorological Society, Boston, pp. 219–222.

Koeppe, C.E., De Long, G.C., 1958. Weather and Climate. McGraw-Hill, New York, Toronto, London, 341 pp.

Kustas, W.P., Pinker, R.T., Schmugge, T.J., Humes, K.S., 1994. Daytime net radiation for a semiarid rangeland basin from remotely sensed data. Agric. Forest Meteorol. 71, 337–357.

NCDC (National Climatic Data Center), 1995. Cooperative summary of the day, dataset TD 3200. U.S. Department of Commerce, National Oceanographic and Atmospheric Administration, National Climatic Data Center, Asheville, NC.

NREL (National Renewable Energy Laboratory), 1993. Solar and meteorological surface observation network, 1961–1990. U.S. Department of Energy, National Renewable Energy Laboratory, Golden, CO.

Pinker, R.T., Frouin, R., Li, Z., 1995. A review of satellite methods to derive surface shortwave irradiance. Remote Sensing Environ. 51, 108–124.

Piper, S.C., 1995. Construction and description of a gridded global dataset of daily temperature and precipitation for terrestrial biospheric modelling. S.I.O. Reference Series No. 94-13, Scripps Institute of Oceanography, University of California, San Diego.

Running, S.W., Nemani, R.R., Hungerford, R.D., 1987. Extrapolation of synoptic meteorological data in mountainous terrain and its use for simulating forest evaporation and photosynthesis. Can. J. Forest Res. 17, 472–483.

Sellers, P.J., 1992. Biophysical models of land surface processes. In: Trenberth, K.E. (Ed.), Climate System Modeling. Cambridge University Press, London, pp. 451–490.

Swift, L.W., 1976. Algorithm for solar radiation on mountain slopes. Water Resources Res. 12(1), 108–112.

Thornton, P.E., Running, S.W., White, M.A., 1997. Generating surfaces of daily meteorological variables over large regions of complex terrain. J. Hydrol. 190, 214–251.

VEMAP Members, 1995. Vegetation/ecosystem modeling and analysis project (VEMAP): comparing biogeography and biogeochemistry models in a continental-scale study of terrestrial ecosystem responses to climate change and CO_2 doubling. Global Biogeochemical Cycles 9, 407–437.